Since January 2020 Elsevier has created a COVID-19 resource centre with free information in English and Mandarin on the novel coronavirus COVID-19. The COVID-19 resource centre is hosted on Elsevier Connect, the company's public news and information website.

Int. J. Electron. Commun. (AEÜ) 120 (2020) 153207

Contents lists available at ScienceDirect

International Journal of Electronics and Communications (AEÜ)

journal homepage: www.elsevier.com/locate/aeue

Regular paper

A *Jia*-shaped artistic patch antenna for dual-band circular polarization

Kwok L. Chung [a], Xiaoqing Yan [a], Yansheng Li [b], Yingsong Li [c,*]

[a] Civionics Research Laboratory, Qingdao University of Technology, Qingdao 266033, China
[b] School of Information and Control Engineering, Qingdao University of Technology, Qingdao 266520, China
[c] College of Information and Communication Engineering, Harbin Engineering University, Harbin 150001, China

ARTICLE INFO

Article history:
Received 18 March 2020
Accepted 12 April 2020

Keywords:
Artistic patch antenna
Kanji patch antenna
Circular polarization
L-shaped feeding probe

ABSTRACT

This article presents a novel single-feed circularly polarized patch antenna for dual-band (2.6 and 3.4 GHz) applications. Details of the design procedure and design considerations of the proposed antenna are described. The novelties of the proposed antenna are counted by (*i*) a meaningful *Jia*-shaped patch used as the primary radiator; (*ii*) a 3D *L*-shaped feeding probe used to excite the stacked patches so that the near degenerate-modes are excited at the desired dual band; (*iii*) down-tilt beams achieved that are particularly suitable for wall-mount base-stations. The measured 3-dB axial-ratio bandwidths are 2.41–2.61 GHz and 3.25–3.42 GHz, where the maximum gains are recorded as 7.3 and 6.3 dBic, respectively. Methods for the adjustment of band ratio down to 1.18 are discussed. The overall antenna size is $100 \times 100 \times 12.8$ mm^3.

1. Introduction

Universally, all humans and animals have a home on earth. We are saddened knowing that many people and animals have lost their *homes* in the recent catastrophic Australian bushfires [1]. Frustrations are felt knowing children, anti-government demonstrators, in Hong Kong destroyed their parent-built *homes* in the past months [2]. Home means sanctuary, the place we can rest, learn, and enjoy time with family. No matter what place you call home, the term strikes a chord deep inside each of us. We all value *home*, which is "家" in Chinese, its mandarin pinyin is "*Jia*".

As a Chinese tradition, everyone unloads their daily work and returns *home* for family reunion and celebrate the Chinese New Year. The authors were drafting this manuscript on the dates just about weeks ahead of the festival. It is therefore very meaningful to have the Chinese character *Jia*-shaped patch antenna presented in this article. The patch antennas embed Chinese character(s) into the antenna design, combining Chinese culture and antenna technology to realize the application of hidden antenna technology [3–12] that is suitable for indoor wireless communications to date. Chinese hieroglyphs are the crystallization of the wisdom of the Chinese nation. They are a kind of inheritance, the most vivid and the most well preserved characters of the ancestors, and are their original way of describing things. A novel wideband Wang-shaped patch array was initially proposed in [4], whereas the Zhong- and the Guo-shaped artistic patch antenna were studied and developed in various contributions [5–9]. Later on, the two-element Zhong-Guo array was also presented with good radiation characteristics [10,11]. *Jia* (家) is a hieroglyphic character and consists of two radicals. Its exterior part is shaped like a house roof at the top, whereas the inner part looks like a hog. The development of the ancient times was low, the chance of hunting and preying was great, and life was not guaranteed. People raised hogs in the house to prepare for food and prevent famine. As such, a hog is symbolized in the house.

Circularly polarized (CP) antennas have been widely installed in modern communication systems due to their anti-fading and anti-interference abilities in a multipath, dense environment. In the past decades, numerous antennas were proposed for dual-band CP operations [13–19]. In 2001, a dual-band CP radiation was achieved by inserting four T-shaped slits at the edges of a single-feed square patch [13]. A S-shaped slotted square patch was proposed for GPS applications [14], where a small frequency-band ratio of 1.28 was attained. In [15], a pair of *L*-shaped stubs was loaded outside a truncated square patch fed by a meandering probe, so that a pair of orthogonal modes can be created for dual band unidirectional radiation. Besides, the dual band ratio can be different by adjusting the stub lengths. In [16], a rotated rectangular patch stacked with a circular patch excited by aperture feed was presented for dual-band CP (2.26/2.67-GHz) operation. A dual-band (0.92/2.45-GHz) RFID antenna comprises two stacked ring-patches excited by a hybrid complicated feed network was introduced [17]. Moreover, an EBG resonator antenna was

* Corresponding author.
E-mail address: liyingsong@ieee.org (Y. Li).

https://doi.org/10.1016/j.aeue.2020.153207
1434-8411/

proposed for dual-band CP (9.65/11.75-GHz) operation [18]. A modified stacked patch with dual band (1.62/2.49-GHz) and dual sense was proposed for BeiDou navigation systems [19], wherein a small antenna profile was accomplished. In [20], a dual-band CP reconfigurable antenna was proposed by using a novel dual-layer metasurface, whereas a wideband CP (3-dB axial ratio bandwidth of 70%) reconfigurable antenna was presented in [21]. However, these aforementioned dual band or wideband CP antennas were not the artistic antennas. The artistic patch antennas such as the Chinese-character-shaped patch antennas imposed additional design constraints from the character shapes. Hence, the design of artistic antennas becomes more challenge.

In this paper, a highly asymmetric *Jia*-shaped artistic patch antenna is introduced for dual-band CP applications. The novelties of the proposed work are: (*i*) an evocative *Jia*-shaped copper patch was used as the radiating element; (*ii*) a 3D *L*-shaped feeding probe was used for enhancing feed-to-patch coupling.

2. Antenna geometry and working mechanism

The *Jia*-character shaped patch was printed in standard SimHei font on the topside of a 0.5-mm thick dielectric substrate RO4003C (ε_r = 3.38, tanδ = 0.0027), as shown in Fig. 1. The *Jia*-character was developed as a type of pictographic characters so that its shape has an irregular yet asymmetrical geometry about *x*- or *y*-axis. The *Jia*-shaped patch was printed using a 0.035-mm thin copper-foil. It has an overall (point-to-point) size of 79.2 mm (W1) and 80 mm (W2) in a near-square grid. A rectangular patch (*R*-patch) of size of *Ra* × *Rb* was printed on the bottom-side of the dielectric substrate. Namely, the *Jia*-patch was arranged to stack on top of the *R*-patch (Fig. 1). The dielectric substrate was suspended over the copper ground plane of size of 100 mm × 100 mm at a height of *H*. The geometric description of the artistic shape of *Jia*-patch was managed by using the coordinate vertex [22], with respect to the geometrical center (0, 0) of the *R*-patch, as shown in Fig. 1. The detailed geometrical parameters and coordinate points (vertexes) are summarized in Table 1. These implicitly give the relative position between two patches. To facilitate the effective feed to patches' coupling using a single feed, a novel 3D *L*-shaped feeding probe was delicately included to capacitively excite the patches via an air-gap (*g*). The relative position between the patches and the feed location (*fp*) were optimized with respect to the center of

Table 1
Geometrical parameters.

Para/Vertex	Value (mm)	Para/Vertex	Value (mm)
W1	79.2	W2	80
Ra	27.3	*Rb*	43.3
1	(4.2, 49)	14	(33.3, 10.5)
2	(−4, 46.9)	15	(26.4, 16.7)
3	(−1, 39)	16	(38.1, 22.3)
4	(−34.7, 39)	17	(−27.7, 20.7)
5	(−34.7, 20.7)	18	(−19.9, 28.1)
6	(−36.1, 5.8)	19	(24.9, 20.2)
7	(−35.9, −9.3)	20	(4.9, 20.3)
8	(−36.8, −23.1)	21	(−4, 20.3)
9	(−7.4, −23.6)	22	(−6.5, 10.9)
10	(−4.4, −31)	23	(−3.3, 7.2)
11	(36.2, −26.1)	24	(0.3, 2.7)
12	(42.5, −19.4)	25	(3, −1)
13	(21.2, 3.7)	26	(4.9, −7.2)
θ	45°	*fp*	(13, −12)
H	11.8	*g*	2.3
Fh	10	*Fv*	9.5

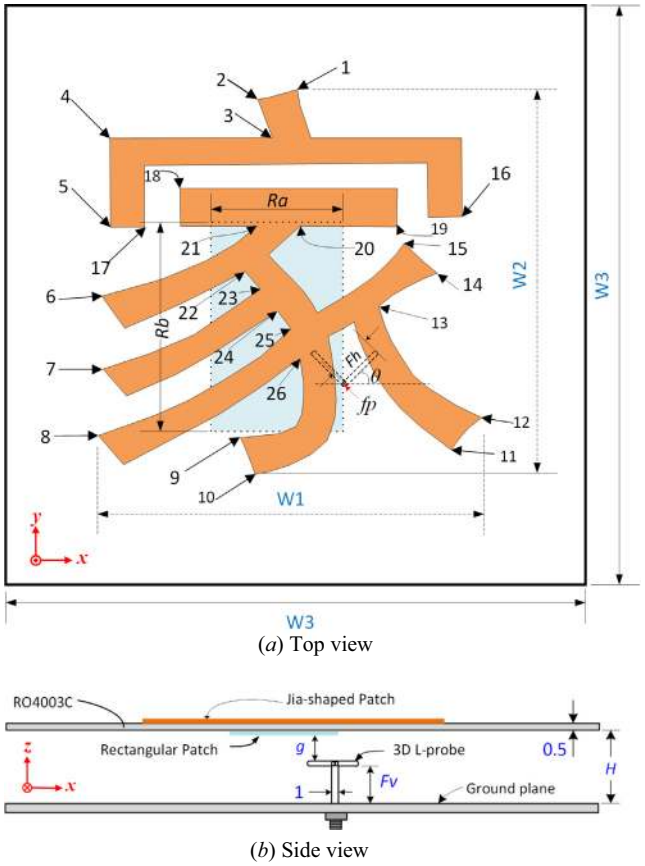

(*a*) Top view

(*b*) Side view

Fig. 1. Geometry of *Jia*-shaped artistic patch antenna.

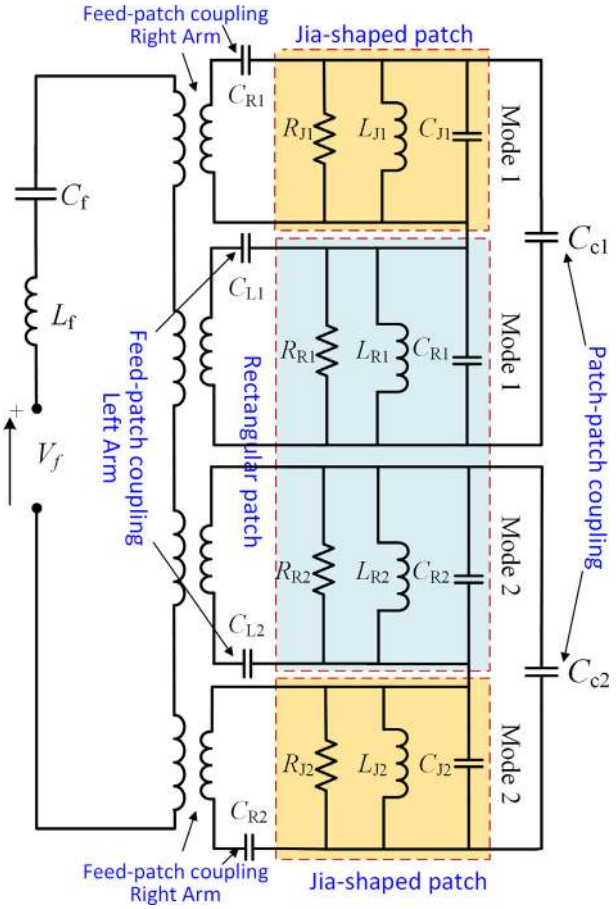

Fig. 2. Equivalent circuit of *Jia*-shaped patch antenna fed by a 3D *L*-probe.

the *R*-patch. The 3D *L*-probe consists of two equal-length horizontal arms (denoted *left-* and *right*-arm) placed orthogonal each other, whereas its right arm is oriented at an angle (θ) with respect to *x*-axis.

In order to generate CP wave using single feed, the horizontal and vertical components (E_φ & E_θ) of the electric field emitted from the *Jia*-patch at each center frequency have to be equal in amplitude with a phase difference of 90° or 270°. Based on this principle, the feed position of the 3D *L*-probe was optimized to obtain the high-low axial ratios below 3-dB. Namely, two pairs of near degen-

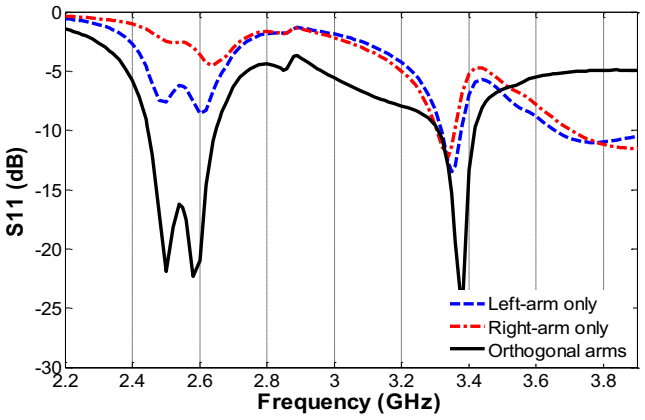

Fig. 3. Comparison of impedance matching in term of S11 between conventional and 3D *L*-probe.

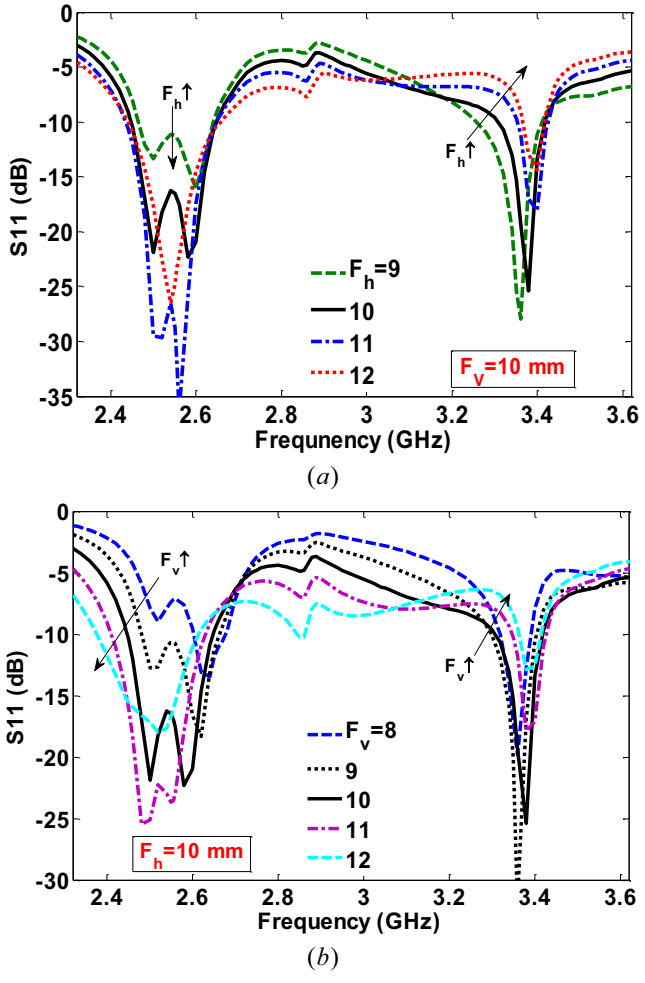

Fig. 4. S11 performance of the initial combinations on different *F*h and *F*v: (*a*) *F*h varies from 12 down to 9 whereas *F*v = 10 mm; (*b*) *F*v varies from 8 up to 12 mm whereas *F*h = 10 mm.

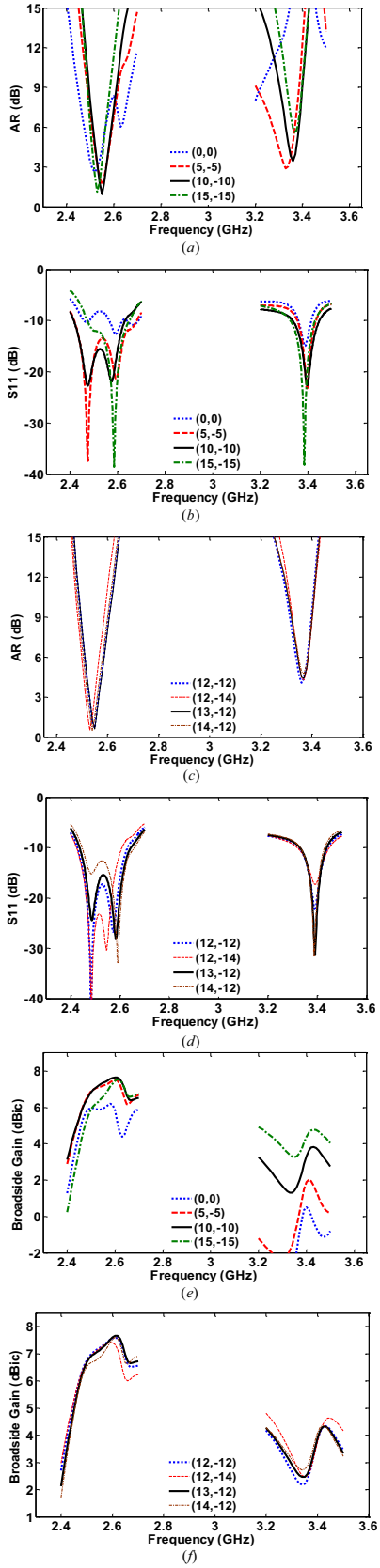

Fig. 5. Coarse and fine search of best feed location: (*a*), (*c*) AR, (*b*), (*d*) S11, and (*e*), (*f*) BG.

erate orthogonal modes were generated independently at the desired center frequencies. The *Jia*-patch is mainly liable for the creation of lower band emission whereas the *R*-patch is responsible for the higher band generation. We may consider that the irregular shape of the *Jia*-patch has negative perturbations removed from a near-square patch. Meanwhile, the left arm of the 3D *L*-probe is liable for the feed of *R*-patch and the *Jia*-patch, whereas the right arm is solely coupled to the *Jia*-patch (Fig. 1). An equivalent circuit was developed to illustrate the coupling mechanism of the artistic antenna as shown in Fig. 2, wherein the Mode 1 and Mode 2 represent the pairs of orthogonal modes of the patches. The use of orthogonal arms was deliberate to raise the effective coupling between the feed and the patches. A comparison of impedance matching using 3D *L*-probe is shown in Fig. 3, where the S11 performance of the 3D *L*-probe outperforms the conventional *L*-shaped feeding probes [23–25].

3. Antenna design procedure

In this section, we describe the stepwise design procedure for the dual-band *Jia*-shaped patch antenna. The goal was to produce an indoor base-station antenna operating at the 5G frequency bands. The design and optimization were undertaken by using Microwave Studio [26]. The stepwise design procedure is presented as follows:

Step 1: outline the *Jia*-character using SimHe font, with its height (W2) approximately equal to 0.6 $\lambda_{2.6G}$ and set the length (*Rb*) of the *R*-patch roughly to 0.5 $\lambda_{3.4G}$, where $\lambda_{2.6G}$ and $\lambda_{3.4G}$ are free-space wavelengths at 2.6 and 3.4 GHz, respectively. Initially, two patches are arranged as stacked patches with their geometrical centers coincided. In Section 4, we will show the dual-band ratio can be primarily set by these patch sizes independently, as well as the relative position.

Step 2: design the 3D *L*-probe. This includes the probe height (*Fv*), length of horizontal arms (*Fh*) and its orientation with respect to *x*-axis (θ). Initially, the total length of *L*-probe (*Fv* + *Fh*) was set approximately to the quarter-wavelength of the high-band frequency, viz., $\frac{1}{4}\lambda_{3.4G} \sim 22$ mm whereas the overall antenna height (*H*) was limited at 12 mm (~$0.1\lambda_{2.6G}$). Fig. 4 displays the antenna performance for a number of combinations on different lengths.

Step 3: search the best feed location (*w.r.t. R*-patch center) of the 3D *L*-probe. The challenge here is the simultaneous accomplishment of the possible lowest ARs at 2.6 and 3.4 GHz. In order to obtain the desired right-hand co-polarization, we search the feed location starting from the patch center (0, 0) along the −45° diagonal-line in four steps till (15, −15). Fig. 5 displays the corresponding variations on AR, S11 and broadside gain (BG). As observed, the feed location affects essentially the AR and gain level in the higher band (3.4 GHz), but the S11 in the lower band (2.6 GHz). Based on the performance trade-offs, as shown in Fig. 5(a)–(f), we further search the best feed location within the range of (12, −12) and (15, −15) by using a fine increment of 1 mm. Four locations were selected to display in Fig. 5(c), (d) and (f) for comparison. As observed, the AR performance of high-low band are almost unchanged (Fig. 5(c)), whereas the BG also showed limited variation (Fig. 5(f)). However, the S11 performance changed considerably in the lower band. Based on these results, the best feed location was determined as *fp* = (13, −12).

Step 4: using the parameters obtained from the above steps, we search the best feed-arm orientation. As described in Section 2, the 3D *L*-probe composed of two orthogonal horizontal arms, so that the coupling areas are higher than the 1D counterpart. As a result, the impedance matching and the broadside gain would be easier to achieve and also higher. However, it is important to obtain the best orientation of the arm position, which essentially controls the level of feed coupling. The horizontal arms were initially oriented at θ = 45° (Fig. 1). Let the rotation angle be α, Fig. 6 shows the six

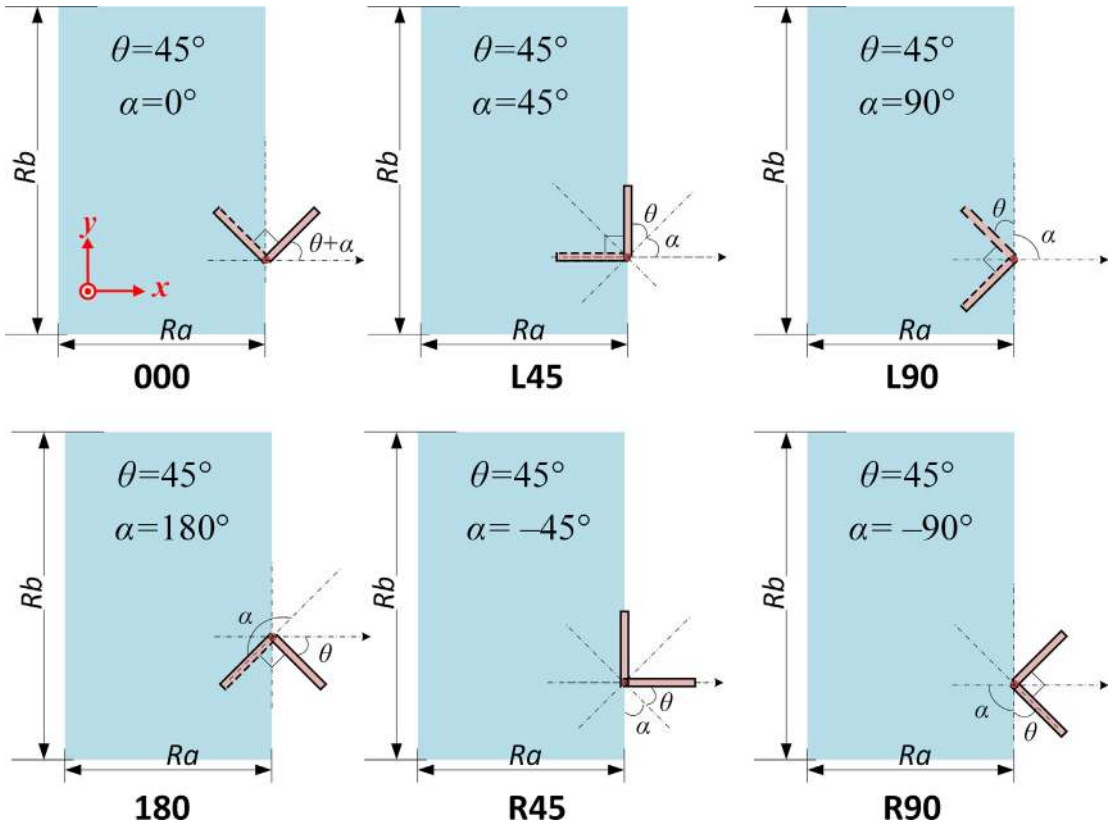

Fig. 6. Arrangement of six different feed-arm orientations.

possible rotations 000, L45, L90, R45, R90 and 180, as α = 0°, 45°, 90°, −45°, −90° and 180°, respectively. When α = 180°, the *L*-probe orientation is principally placed upside down. Fig. 7 shows the corresponding antenna performance in terms of AR, BG and S11. As demonstrated, the best feed orientation can be determined as 000 (α = 0°). Besides, minimal coupling was observed under the cases of R45 (α = −45°) and R90 (α = −90°), where both the BG and S11 in the lower band were deteriorated.

4. Design consideration on essential parameters

In this section, we present the results for a series of design considerations on the essential geometrical parameters of the proposed antenna. The aim is to have an in-depth understanding of the working mechanism of the 3D *L*-probe fed patch antenna and pursuit the best parameters for desired antenna performance. This study can also provide an effective way on the fine tuning of the desired performance.

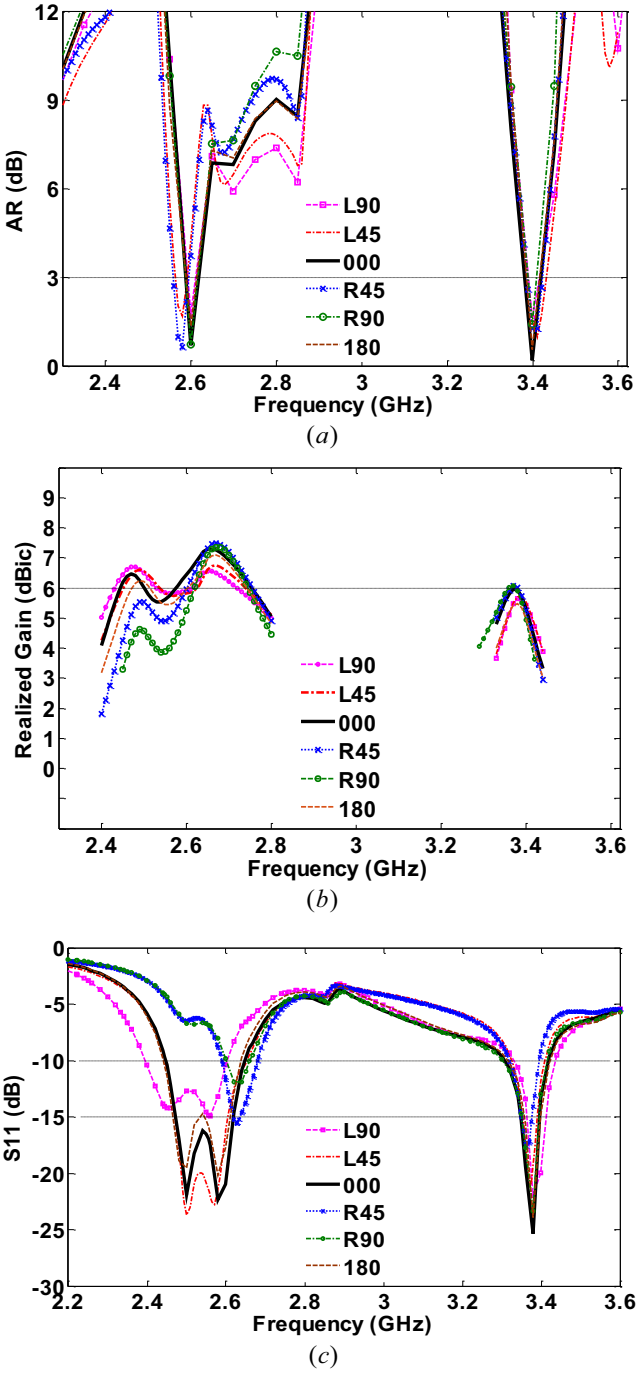

Fig. 7. Antenna performance under different orientations of 3D *L*-probe: (*a*) AR, (*b*) BG, (*c*) S11.

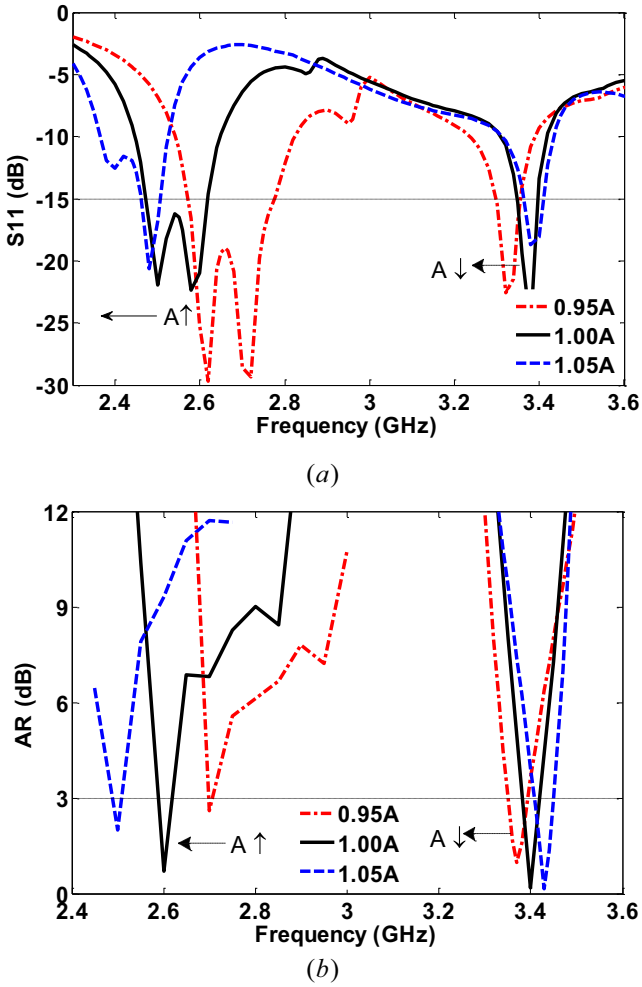

Fig. 8. Effects of *Jia*-shaped patch size on (*a*) S11 and (*b*) AR.

4.1. Consideration of Jia-shaped patch size

The size of the *Jia*-patch was changed, and the product of the widest transverse distance (W1) and the widest vertical distance (W2) was used as a representation of the overall area of *Jia*-shaped patch. Namely, **A** = W1 × W2. With reference to Table 1, we adjusted **A** by ± 5% to observe the variation of antenna performance while other parameters reminded unchanged. Fig. 8 shows the effects of **A** on S11 and AR. As predicted, the overall size of *Jia*-patch (**A**) affects the center frequency of the lower band considerably than the higher band. In particular, a 5% increase of **A** gives the center frequency of AR shift-down about 100 MHz, but a minor effect in the high band.

4.2. Adjustment of rectangular patch size

Setting **B** is the area (*Ra* × *Rb*) of *R*-patch and was adjusted by ±5% to observe the variation of antenna performance while other parameters reminded unchanged. Fig. 9 demonstrates its effects on S11 and AR, whereas Fig. 10 displays the BG variations when

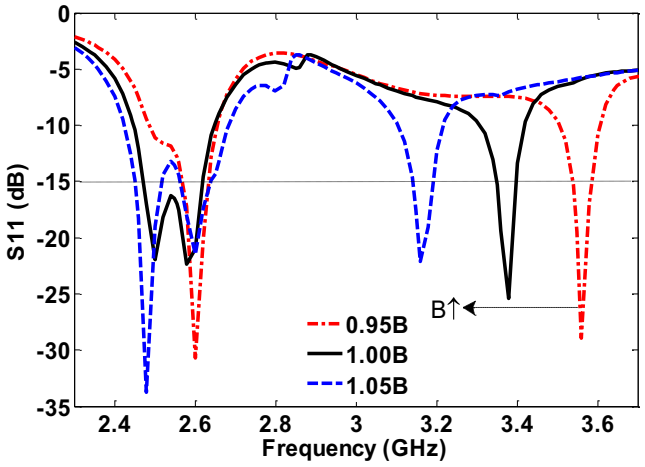

(a)

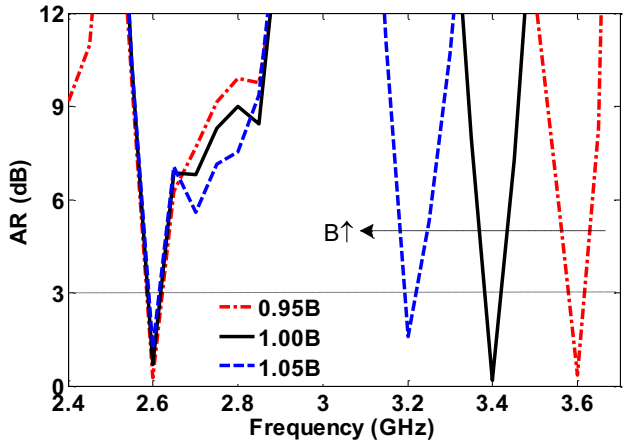

(b)

Fig. 9. Effects of rectangular patch size on (*a*) S11 and (*b*) AR.

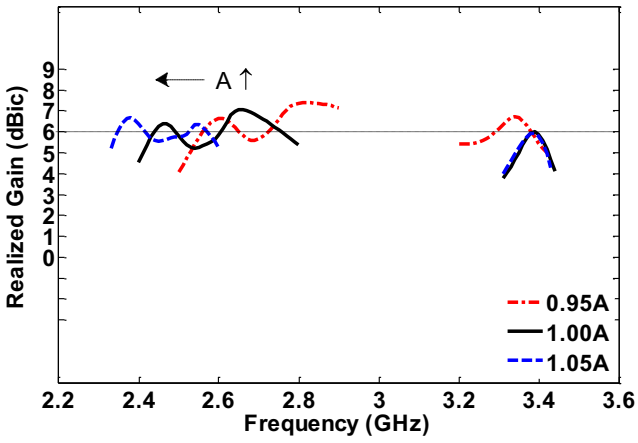

(a)

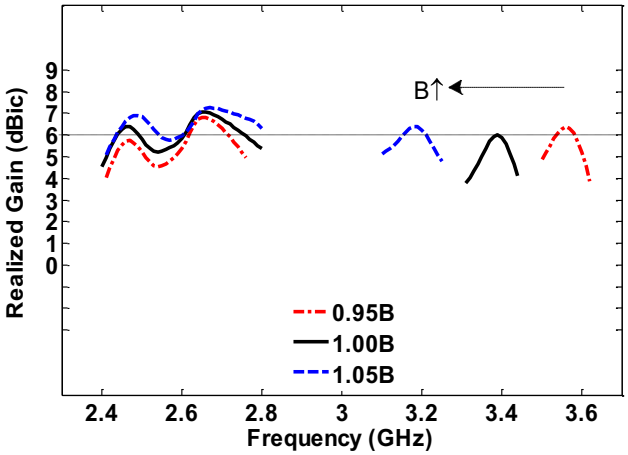

(b)

Fig. 10. Effects of patch sizes on BG: (*a*) *Jia*-patch, (*b*) rectangular patch.

sizes **A** and **B** were changed, independently. It can be seen that the *R*-patch size has no significant effect in the lower band but has a great impact in the high-band performance. In particular, the AR frequency band moves to the low frequencies by 200 MHz as the patch size **B** increases by 5%. It is concluded that the higher frequency band (3.4 GHz) is mainly derived from the *R*-patch size, whereas the lower band (2.6 GHz) is determined by the *Jia*-patch size **A**.

4.3. Effects of relative position between two patches

Select a coordinate from the *Jia*-shaped patch, say (U_b, V_b), we moved the *Jia*-patch left-and-right and up-and-down by 1 mm along with *x*- and *y*-axis, respectively. Fig. 11 displays the corresponding variations on AR and S11 performance in four cases. We observed that, in general, the affection in the high band performance is more sensitive than the lower band. In particular, the *on-axis* AR performance. When the *Jia*-patch moved to right by 1 mm, the lowest AR changes whereas their frequencies shift down by 20–30 MHz. Moreover, ARs went up with decreased frequencies as the *Jia*-patch moved up by 1 mm (Fig. 11(b)). For S11 performance, the high-band performances are more sensitive in the movement along *y*-axis. The high-band resonant frequency shifts down when the *Jia*-patch moved upward, as shown in Fig. 11(d). These indicate that the small adjustment of relative position provides another way for the fine adjustment of the band ratio.

4.4. Consideration of air-gap length

With reference to Figs. 1 and 2, the air-gap (*g*) between the feed-arms and the *R*-patch essentially controls the magnitude of the capacitance C_{L1}, C_{L2}, C_{R1} and C_{R2}. Namely, the coupling from the feed to the patches, it is another important parameter that affects the antenna performance. Fig. 12 displays its effects on S11 and AR when g = 1.3, 2.3 and 3.3 mm, respectively. As observed, the magnitude of air-gap affects the S11 at the high and low band and hence the BG (not shown), but has insignificant effect on AR. The AR curves shown in Fig. 12(b) are virtually unchanged.

4.5. CP handedness realization

With reference to the equivalent circuit of the dual-band *Jia*-patch as shown in Fig. 2, there are two theoretical conditions for creation of dual-band circular polarization in the maximum radiation direction. One is the necessary condition that the magnitudes of electric field components ($E_\varnothing$, E_θ) must be equaled in the dual band, whereas the second one is the sufficient condition that their phase difference must be ±90°. When the phase of $E_\varnothing$ leads E_θ by +90°, a left-hand CP is produced. Conversely, when $E_\varnothing$ lags E_θ by 90°, a right-hand (RH) CP is created. Fig. 13 plots the simulation results of these E-field components both in magnitude ratio and phase difference at the lower (2.6 GHz) band and the upper

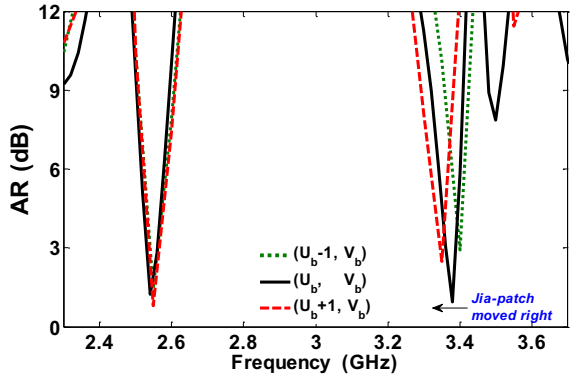

(*a*)

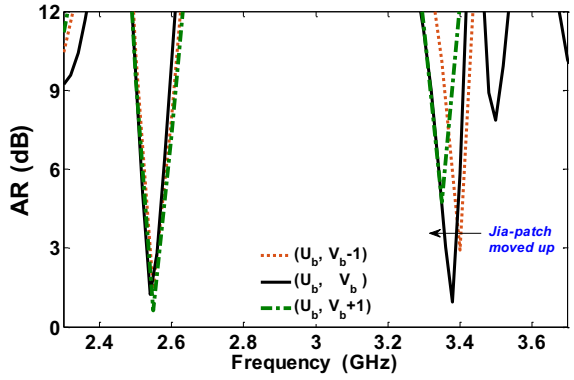

(*b*)

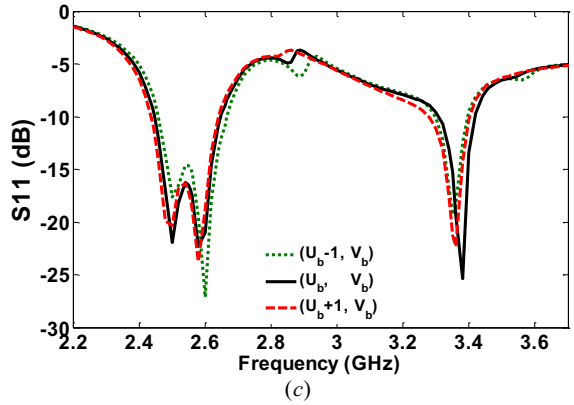

(*c*)

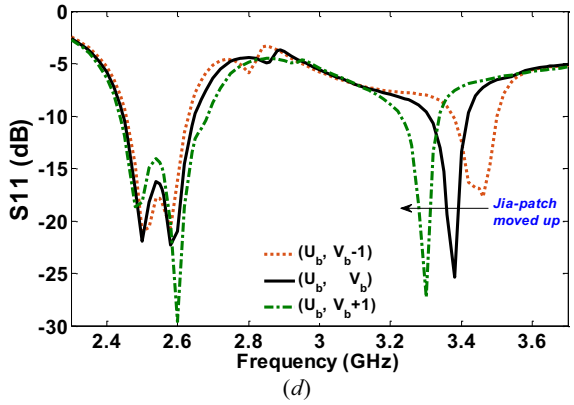

(*d*)

Fig. 11. Effects of relative position between patches on (*a*)–(*b*) AR and (*c*)–(*d*) S11.

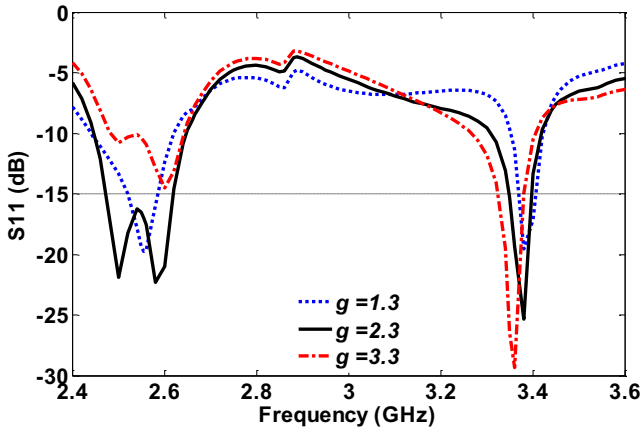

(*a*)

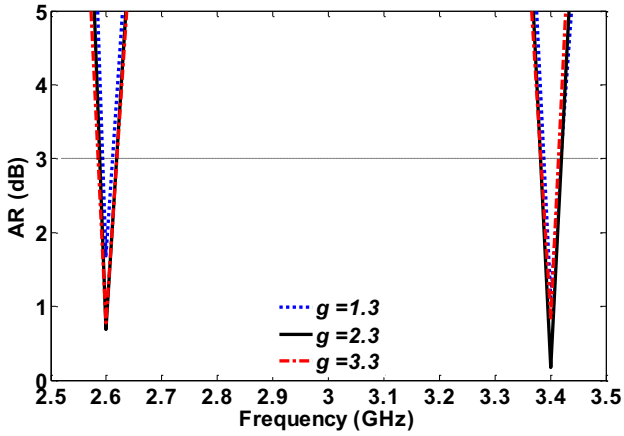

(*b*)

Fig. 12. Effects of air-gap length on (*a*) S11 and (*b*) AR.

(3.4 GHz) band. From these plots we know that the RHCP is generated in both the bands.

5. Experimental verification

To validate the working mechanism as described, the proposed dual-band *Jia*-shaped patch antenna was fabricated and its overall performance was measured. As a common practice, the reflection coefficient (S11) was measured before the measurement of far-field performance took place. S11 was undertaken by using the Keysight performance network analyzer N5222A, whereas the measurement of far-field performance metrics was carried out inside the near-field chamber SATIMO StarLab at the Qingdao University of Technology. Fig. 14 displays a photograph of the *Jia*-shaped patch antenna that was under measurement in the chamber, whereas the radiation patterns in two principal planes/-cuts are shown in Fig. 15, wherein the simulated patterns were verified by the measured ones. As seen, the RHCP co-polarization were obtained in the desired dual frequency band, which are corroborated with the prediction from the simulation. Moreover, the maximum power directions of the main beams in the elevation (*yz*) plane are pointing to 15° (Fig. 15(b)) and 18° (Fig. 15(d)) in the low- and high-band, respectively. As a result, this artistic patch

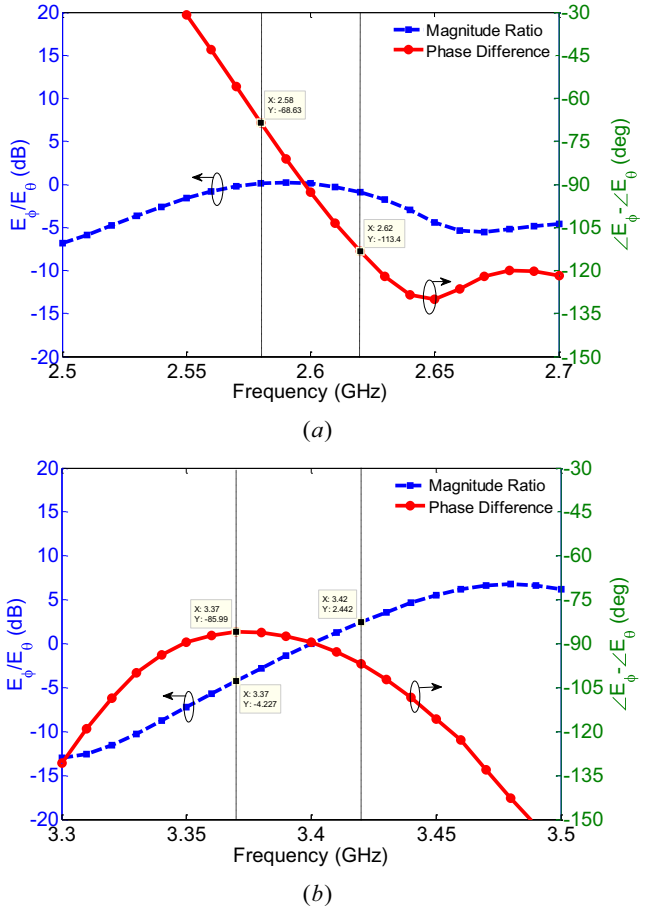

Fig. 13. Computed ***E***-field magnitude ratio $|E_{\varnothing}/E_{\theta}|$ and phase difference $\angle E_{\varnothing} - \angle E_{\theta}$ of the Jia-shaped patch in (*a*) lower band and (*b*) upper band.

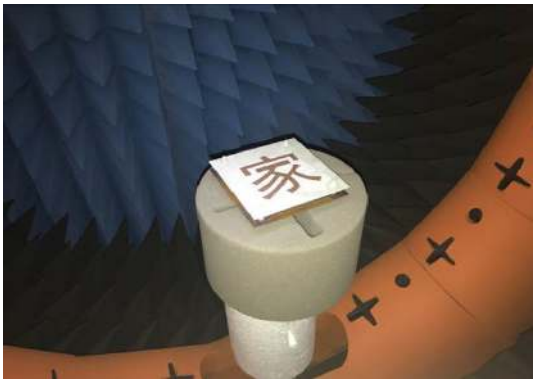

Fig. 14. Photograph of a fabricated dual-band *Jia*-shaped patch antenna under measurement.

antenna exhibits the down-tilt beams in the dual band. This feature is highly desired for wall-mounted antennas, where additional mechanical tilting/mounting is not required during the installation. Indeed, this is one of the by-products from the Chinese-character-shaped patch antennas [5].

Fig. 16 displays the other performance metrics verified by the measurement results. In general, excellent agreements were attained. Small discrepancies inevitably emerged mainly owing to unexpected tolerances in antenna fabrication. The dual-band axial ratio was measured from 2.58 to 2.62 GHz and 3.37 to 3.42 GHz, wherein the maximum gains were recorded as 7.3 and

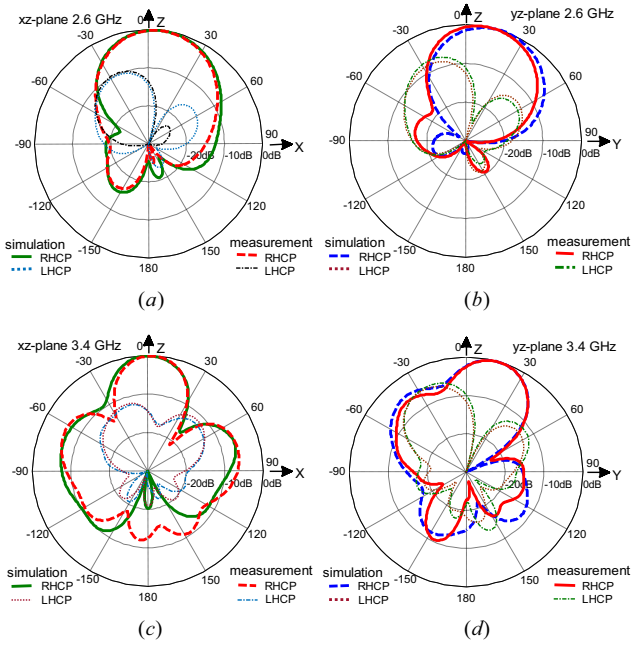

Fig. 15. Simulated and measured radiation patterns in *xz*- and *yz*-plane: (*a*) 2.6 GHz, (*b*) 3.4 GHz.

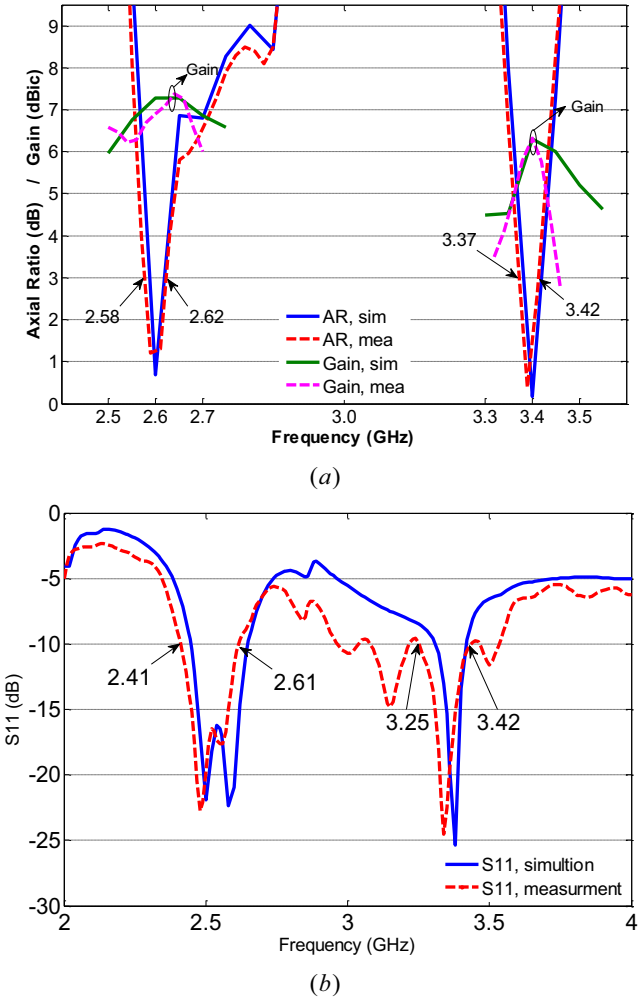

Fig. 16. Simulated antenna performance verified by measurement: (*a*) AR and gain, (*b*) S11.

6.3 dBic for the low- and high-band, respectively. Meanwhile, the reflection coefficient plots (Fig. 16(b)) indicate that the dual impedance bandwidth was measured from 2.41 to 2.61 GHz and 3.25 to 3.42 GHz, respectively, which sufficiently covers the axial-ratio bandwidths.

In addition, this CP artistic patch antenna would be the first dual-band one in literature, no comparable performance is available.

6. Conclusions

The Chinese characters are profound. *Jia* means home in Chinese. Home gives importance in our life, as a recent example, home is a best place of isolation from the outbreak of novel coronavirus-2019 (COVID-19). This article presents a novel *Jia*-shaped patch antenna printed in standard SimHei font for dual-band circular polarization at 2.6 and 3.4 GHz. A detailed design procedure as well as the working mechanism were described, in particular, the creation of pairs of near degenerate-orthogonal modes was achieved, such that a dual axial-ratio (3-dB) bandwidth was produced at 2.58–2.62 GHz and 3.37–3.42 GHz, wherein the maximum gain of 7.3 and 6.3 dBic was obtained, respectively. Moreover, the dual-band ratio of this artistic patch antenna can be adjusted by (*i*) changing the patches' sizes, and (*ii*) the relative position of the stacked patches. The parametric study indicates that when the *Jia*-patch size reduced by 5% and the rectangular patch size increased by 5%, the dual-band ratio can be reduced to 1.18. Finally, the down-tilt radiation is also a special feature of the proposed dual-band antenna.

Declaration of Competing Interest

The authors declare that they have no known competing financial interests or personal relationships that could have appeared to influence the work reported in this paper.

Acknowledgement

This work was supported by the 2019 Key Research & Development Plan of Shandong Province, P. R. China. Grant No. 2019GGX101059.

References

[1] Reuters, Australia's bushfires circle Sydney as temperatures soar; 2019, Dec 21. [Online]. Available: http://www.msn.com/en-us/news/world/update-4-australias-bushfires-circle-sydney-as-temperatures-soar/ar-BBYdbWe.
[2] France 24, Hundreds of shops destroyed as Hong Kong protesters defy rally ban; 2019, Oct 20. [Online]. Available: https://www.france24.com/en/20191020-hundreds-of-shops-destroyed-as-hong-kong-protestors-defy-rally-ban.
[3] Wang Weimin, Ran Juqing, Hu Nan, Xie Wenqing, Wu Yongle, Kishk Ahmed A. A novel differential filtering patch antenna with high selectivity. Int J RF Microw Comput Aided Eng 2019;29(10). https://doi.org/10.1002/mmce.v29.1010.1002/mmce.21880.
[4] Chung KL, Li Y, Zhang C. Broadband artistic antenna array composed of circularly-polarized Wang-shaped patch elements. AEU Int J Electron Commun 2017;74:116–22. https://doi.org/10.1016/j.aeue.2017.02.006.
[5] Wang L, Liu R, Li W, Xie S, Chung KL. Kanji patch antenna. In: 2019 international workshop on electromagnetics: applications and student innovation competition (iWEM); 29–31 Aug 2018. Nagoya, Japan. Nov 2018. https://doi.org/10.1109/iWEM.2018.8536646.
[6] Niu Z, Zhang H. Isolation enhancement in Chinese character antenna array using simple defect ground structure. Int J RF Microw Comput Aided Eng. 2019;29:e21927. https://doi.org/10.1002/mmce.21927.
[7] Li W, Chung KL, Liu R. A Zhong-shaped patch antenna. In: IEEE international conference on signal processing, communications and computing (ICSPCC) 2018. Qingdao; Sep. 14–17, 2018. p. 1–4.
[8] Chung KL, Cui A, Feng B. A Guo-shaped patch antenna for hidden WLAN access points, submitted to International Journal of RF and Microwave Computer-Aided Engineering; 13 Feb 2020.
[9] Chung KL, Liu R, Li W, Lai J, Feng B. On the circular-polarization operation of Chinese-character-shaped patch antenna. In: 11th intern conference on microw. MM-wave technology (ICMMT2019) Guangzhou, China; May 19–22. 2019.
[10] Chung KL, Li W, Li Y. Chinese character-shaped artistic patch antenna. IEEE Antennas Wireless Propag Lett 2019;18(8):1542–6.
[11] Chung KL, Li W, Li Y. A study on inter-element spacing of Chinese-character-shaped patch antenna array. In: 2019 cross strait quad-regional radio science and wireless technology conference (CSQRWC2019) Taiyuan, China; July 18–21, 2019.
[12] Jiang J, Xia Y, Li Y. High isolated X-band MIMO array using novel wheel-like metamaterial decoupling structure. Applied Computational Electromagnetics Society Journal 2019;34:1829–36.
[13] Yang KP, Wong KL. Dual-band circularly-polarized square microstrip antenna. IEEE Trans Antennas Propag 2001;49:377–82.
[14] Nasimuddin, Chen ZN, Qing X. Dual-band circularly polarized S-shaped slotted patch antenna with a small frequency-ratio. IEEE Trans Antennas Propag 2010;58:2212–12115.
[15] Chen CH, Yung EKN. A novel unidirectional dual-band circularly-polarized patch antenna. IEEE Trans Antennas Propag 2011;59:3052–7.
[16] Deng CJ, Li Y, Zhang ZJ, Pan GP, Feng ZH. Dual-band circularly polarized rotated patch antenna with a parasitic circular patch loading. IEEE Antenna Wirel Propag Lett 2013;12:492–5.
[17] Liu Q, Shen JY, Liu HL, Liu YA. Dual-band circularly-polarized unidirectional patch antenna for RFID reader applications. IEEE Trans Antennas Propag 2014;62:6428–34.
[18] Zeb BA, Nikolic N, Esselle KP. A high-gain dual-band EBG resonator antenna with circular polarization. IEEE antenna wirel Propag Lett 2015;14:108–11.
[19] Yang HC, Fan Y, Liu XY. A compact dual-band stacked patch antenna with dual circular polarizations for Beidou navigation satellite systems. IEEE Antenna Wirel Propag Lett 2019;18:1472–6.
[20] Chen XF, Zhao YJ. Dual-band polarization and frequency reconfigurable antenna using double layer metasurface. Int J Electron Commun (AEU) 2018;95:82–7.
[21] Li M, Wu Y, Wang W, Kishk AA. Wideband polarization reconfigurable differential circularly polarized antenna. IEEE Access 2019;7:64697–703.
[22] Chung KL, Xie S, Li Y, Liu R, Ji S, Zhang C. A circular-polarization reconfigurable meng-shaped patch antenna. IEEE Access 2018;6:51419–28.
[23] Luk KM, Mak CL, Chow YL, Lee KF. Broadband microstrip patch antenna. Electron Lett 1998;34(15):1442–3.
[24] Li P, Luk KM, Lau KL. A dual-feed dual-band L-probe patch antenna. IEEE Trans Antennas Propag 2005;53(7):2321–3.
[25] Lau KL, Luk KM. A novel wideband circularly polarized patch antenna based on L-probe and aperture-coupling techniques. IEEE Trans Antennas Propag 2005;53(1):577–80.
[26] CST Microwave Studio. Computer simulation technology, [Online] Available: https://www.cst.com/.